Journal of Applied Polymer Science

Quantification and elucidation of the UV-light triggered initiation kinetics of TPO and BAPO in liquid acrylate monomer

Klaus Ruhland,[1] **Fereshteh Habibollahi**,[2] **Robert Horny**[2]
[1]Institute of Materials Resource Management, University of Augsburg, Universitätsstr. 1, D-86135 Augsburg, Germany
[2]University of Augsburg Institute of Physics, Experimental Physics II, Universitätsstr. 1, D-86135 Augsburg, Germany
Correspondence to: K. Ruhland (E-mail: klaus.ruhland@physik.uni-augsburg.de)

ABSTRACT: The initiation kinetics of two important UV-light-triggered initiators for the radical polymerization [diphenyl-2,4,6-trimethyl benzoyl phosphine oxide (TPO) and phenyl-bis(2,4,6-trimethyl benzoyl) phosphine oxide (BAPO)] has been quantified in dependence on the initiator concentration (0.25–2 mol %), the light intensity at 365 nm (0–2000 mW cm^{-2}), the thickness of the sample (50–200 μm), the temperature (25–80 °C), the monomer [2-ethyl hexyl acrylate (EHA) and 2-ethyl hexyl methacrylate (EHMA)] and the atmosphere (oxygen free and air) directly in the liquid acrylate monomer. The determination of the kinetic parameters was done by applying two independent procedures: (1) following the initiator decay with respect to the irradiation time, evaluated by radiometric measurements of the UV-light absorption at 365 nm and (2) via titration of the initiation process by using defined under-stoichiometric to stoichiometric amounts of TEMPO as inhibitor, evaluated by means of FTIR-ATR spectroscopy. The validity of the titration procedure was proven by means of ^{13}C and ^{31}P NMR studies of ^{13}C-labeled TPO and was explained by a Lewis acid/base interaction between the carbonyl carbon of the initiator and the oxygen of TEMPO. Both methods resulted in very close kinetic parameters. Thus, reliable values for the extinction coefficients ε_{365} at 365 nm, for the effective rate constants of the α cleavage k'_{α} (containing the quantum yield and the initiator efficiency) when dissolved in the liquid monomer could be provided for both initiators for the first time. The effect of dioxygen quenching in dependence of sample thickness and the temperature dependence on the initiation step were evaluated. EHA was compared with EHMA as liquid monomer, and a yet unmentioned inhibition in case of EHMA was discovered. © 2019 The Authors. *Journal of Applied Polymer Science* published by Wiley Periodicals, Inc. J. Appl. Polym. Sci. **2020**, *137*, 48357.

Received 4 July 2019; accepted 18 July 2019
DOI: 10.1002/app.48357

INTRODUCTION

Radical polymerization is among the most important polyreactions in polymer sciences. The initiation of this polyreaction requires the generation of radicals, which can be brought about by means of different external stimuli, in particular by means of heat or UV light. While the thermal initiation is explored very well, and quantitative data for its kinetics are provided in the literature over almost the complete temperature range starting from about 20 °C up to about 290 °C[1–3] (although in general determined for an innocent solvent rather than directly in the liquid acrylate monomer), experimental quantitative data about the initiation kinetics for UV light-triggered systems are still rare.[4] There are several reasons for the discrepancy between these two external stimuli. First, UV-triggered initiation because of its limitation to applications in thin layers is still not used as frequently as thermal initiation (although UV-triggered initiation is becoming more and more important also for industrial applications[5–18]). And second, the quantification of the initiation kinetics is decisively more challenging in case of the UV-light triggered initiators because of the time range (sub-second to second range for UV-light as compared to hours in the case of thermal initiation) and the additional requirement of determining, regulating, and taking into account the UV-light parameters (intensity J, extinction coefficient ε) in comparison to a simple temperature regulation and determination (which itself becomes an additional parameter for the UV-triggered initiation). Another limiting factor of the existing initiation parameters (also for the thermal case) is that the determination is in general performed in

Additional Supporting Information may be found in the online version of this article.

an innocent solvent, while in an application (in particular concerning the UV-triggered initiation), the radical polymerization is done in the solvent-free bulk state.

In our study, we concentrated on two of the most frequently used UV-triggered initiators, namely diphenyl-2,4,6-trimethyl benzoyl phosphine oxide (TPO) and phenyl-bis(2,4,6-trimethyl benzoyl) phosphine oxide (BAPO) (Figure 1), belonging to the group of acyl phosphine oxides which can be α-cleaved in a Norrish-Type I photo-reaction on exposure to defined LED-UV light at 365 nm. Highly sophisticated examinations about the principal initiation mechanism have been published starting from the late 1990s.[19–27]

We have quantified the initiation kinetics for these initiators as function of film thickness d, light intensity J, initiator starting concentration c_A^o, temperature T, and the presence or absence of air and the type of acrylate monomer. As a medium for the examinations we exclusively used mixtures of the initiator directly in the liquid acrylate monomer because these are the conditions under which the initiators are applied in general. As irradiation source an LED with maximum intensity J_{max} of 2000 mW cm^{-2} and sharp emission wavelength distribution of 365 nm ± 5 nm (see Supporting Information Figure S50) was used which could be triggered into rectangular time pulses as short as 20 ms (see supporting information Figures S44–S47). The actual intensity was double checked for each experiment with a radiometer. We quantified the initiation kinetics at defined film thickness by the time-dependent changes of the light absorption via radiometer measurements (initiator decay) and additionally by trapping the radicals with defined under-stoichiometric to stoichiometric amounts of TEMPO as inhibitor via FTIR ATR-spectroscopic measurements (radical formation from the initiator; TEMPO titration), observing the polymerization behavior after defined amounts of short time pulses of irradiation. The TEMPO titration procedure has been carefully examined by additional NMR experiments using ^{13}C-labeled TPO (^{13}C-TPO). The collected experimental data were adjusted to the initiator-specific kinetic models by using POLYMATH as a fitting program for the nonlinear optimization problem.

On doing so, we could provide for the first time quantitative data for the effective rate constant $k_\alpha' = k_\alpha \cdot E_\alpha \cdot Q_\alpha$ (k_α is the rate constant of α-cleavage; E_α is the initiator efficiency; Q_α is the quantum yield of α-cleavage) and for the extinction coefficient ε_{365} of the initiators at 365 nm directly in liquid acrylate monomer. With these parameters in hands, the complete kinetic behavior of these two photo-initiators can now be confidently precalculated for the case of bulk acrylate.

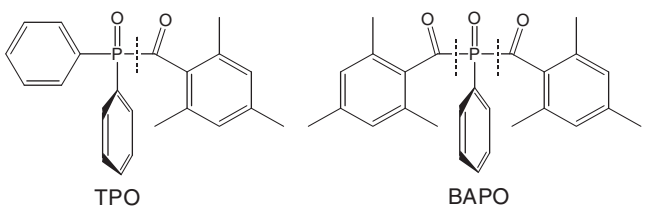

Figure 1. Chemical graphs for the two initiators TPO and BAPO under investigation in this study (dashed lines label the position of α-cleavage).

On examination of a methacrylate in comparison to the analogous acrylate, we could discover a yet unmentioned inhibiting effect of the methacrylate on the initiation process. Also the quenching influence of air in contact with the liquid acrylate and the temperature dependence on the initiation kinetics were elucidated.

The principle procedure to quantify reliably the initiation kinetics for UV-triggered initiators as presented in this contribution can most likely be transferred to several other UV-triggered initiators.

EXPERIMENTAL

Materials

TEMPO (98%, Sigma-Aldrich, Munich, Germany), diphenyl-2,-4,6-trimethyl benzoyl phosphine oxide (TPO, 97%, Sigma-Aldrich, Munich, Germany), phenyl-bis(2,4,6-trimethyl benzoyl) phosphine oxide (BAPO, 98%, Sigma-Aldrich, Munich, Germany), 2,2-diphenyl-1-pikryl hydrazyl radical (DPPH, Sigma-Aldrich, Munich, Germany), Galvanoxyl radical (abcr GmbH, Karlsruhe, Germany), diphenylphosphine oxide (97%, Alfar Aesar, Kandel, Germany), methyl-diphenyl phosphite (98 + %, Alfar Aesar, Kandel, Germany), ^{13}C-sodium carbonate (99% ^{13}C, Sigma-Aldrich, Munich, Germany), oxalyl chloride (98%, Alfar Aesar, Kandel, Germany), acryloyl chloride (>96%, Merck, Darmstadt, Germany), sodium iodide (99.5%, Merck, Darmstadt, Germany), sodium hydride (57–63% oil dispersion, Alfar Aesar, Kandel, Germany), mesityl magnesium bromide (1 M in 2-Me-THF, Alfar Aesar, Kandel, Germany), magnesium sulfate anhydrous (technical grade, AppliChem, Darmstadt, Germany), 2,4,6-trimethyl benzoic acid (99%, Alfa Aesar, Kandel, Germany), sodium thiosulfate anhydrous (99%, Alfa Aesar, Kandel, Germany), sulfuric acid (95–97%, Merck, Darmstadt, Germany) $CDCl_3$ (99.8% D, Deutero GmbH, Kastellaun, Germany), d^3-methanol 99.5% D, Deutero GmbH, Kastellaun, Germany), acetone (98%, VWR, Darmstadt, Germany), were used as received.

Diethyl ether (99.9 + %, VWR, Darmstadt, Germany), toluene (99%, Merck, Darmstadt, Germany), hexane (98.5%, Merck, Darmstadt, Germany), and tetrahydrofurane (THF, 99%, Merck, Darmstadt, Germany) were dried using a two-column drying system (Innovative Technologies, Inc., Hong Kong, China). d^8-Toluene (99.5% D, Deutero GmbH, Kastellaun, Germany) was stored over activated molecular sieves (0.3 nm).

The inhibitor in 2-ethyl hexyl acrylate (EHA, 98%, Sigma-Aldrich, Munich, Germany; 0.001–0.11% mono-methyl ether hydroquinone), 2-ethyl hexyl methacrylate (EHMA, 98%, Sigma-Aldrich, Munich, Germany; 50 ppm mono-methyl ether hydroquinone) and methyl acrylate (MA, 98%, Sigma-Aldrich, Munich, Germany; 100 ppm mono-methyl ether hydroquinone) was removed prior to use by extraction with a 2 N sodium hydroxide solution in water, followed by drying with anhydrous magnesium sulfate and distillation. To check the influence of dissolved oxygen in the monomers, they were degassed by three freeze/pump/thaw cycles with argon as inert gas. No difference was found for these degassed monomers in comparison to the nondegassed ones in our experiments. (However, we note that air on the surface of the acrylate liquid does influence the behavior as it is well known and as will be shown below in this work.)

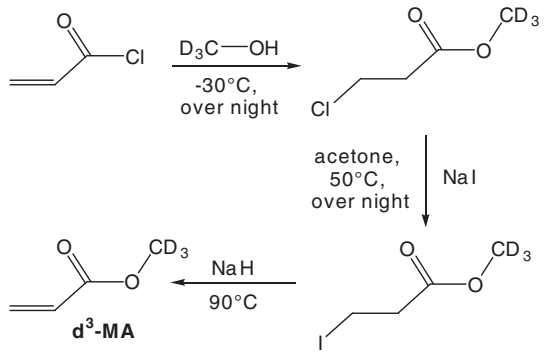

Figure 2. Pathway for the synthesis of d^3-MA.

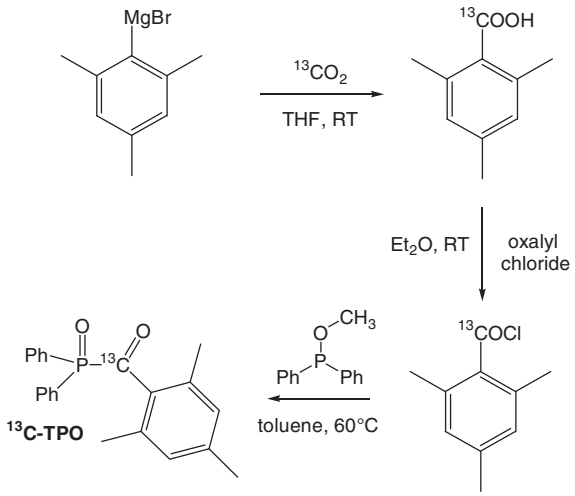

Figure 3. Pathway for the synthesis of ^{13}C-TPO.

Methyl acrylate, deuterated at the methyl group (d^3-MA) which was necessary for the NMR experiments in this work, was synthesized according to Figure 2.

The substitution of chlorine by iodine was necessary because the 3-chloro propionic methyl ester had a too low-boiling point for the last step. For experimental details and characterization data, see the Supporting Information Figures S1–S11.

TPO with ^{13}C-labeling at the carbonyl carbon (^{13}C-TPO) was synthesized according to Figure 3.

The $^{13}CO_2$ for the first step was generated from $Na_2{}^{13}CO_3$ with concentrated sulfuric acid in a separated flask. For experimental details and characterization data, see the Supporting Information Figures S12–S23.

Figure 4 depicts isolated reaction products of the reaction between TPO or ^{13}C-TPO and TEMPO in MA or toluene.

Concerning the procedure of isolation and the characterization data of them, see the Supporting Information Figures S24–S36.

Devices Used in this Work

As UV light source a commercial high power UVA-LED (Nichia SMD LED UV NC4U133B, platine mounted) at peak wavelength of 365 nm was operated by a programmable current sourcemeter (Keithley 2400). Adjustment of current intensities up to the LED specification limit of 700 mA and pulse times down to 20 ms were controlled by a connected PC using a self-written software within a LABWIEW development environment.

Pulse times and current stability was checked with an oscilloscope by measuring the voltage change across a 1.2 Ohm resistor placed in the electrical circuit of current source and LED (see Supporting Information Figures S44–S47). We recognized an additional stabilization time of 1.6 ms, which had to be taken into account.

In addition, we used the voltage signal created by an irradiated Si-photodiode for testing the stability of light emission (which turned out to be rather stable within few percentage during pulse times up to 60 ms).

For the spectral intensity measurements a UV radiometer UVPAD (Fa. Opsytec Dr. Gröbel) was used (spectral range: 200–440 ± 5 nm; resolution: 2 nm; irradiance measurement range: 2–5000 mW cm^{-2}; sampling rate: 10–1000 ms) with a circular sensor area of 3 mm diameter comparable to the lateral dimensions of the FTIR sensor (see also Supporting Information Figure S49).

As ATR/FTIR device served an ALPHA Platinum ATR unit (Fa. Bruker) with diamond crystal. The evaluation of the IR data was done using the software package OPUS 7.2 (see also Supporting Information Figure S48).

A micrometer screw (Fa. Helios) was used to determine the thickness of the glass fibers used as space holder in the experiments (measurement certainty: ± 7 µm).

Devices used for the characterization of isolated and synthesized compounds:

IR measurements were performed using a Thermo Nicolet FT/IR machine (Fa. Nexus) in the ATR modus (diamond crystal) at room temperature and were evaluated using the software package OMNIC 6.1a.

^{1}H, ^{2}H, ^{13}C, and ^{31}P solution NMR data were collected using a Mercury plus400 high- resolution console (Varian/Agilent) with a PFG ATB broadband probe (1H/19F/X 5 mm) and were evaluated using the software package VNMR 2.2a. These NMR measurements were

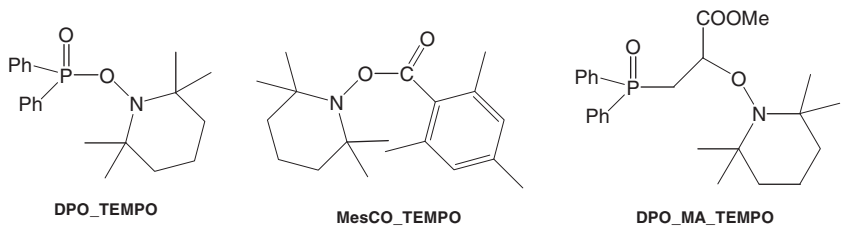

Figure 4. Isolated reaction products of the reaction between TPO or ^{13}C-TPO and TEMPO on irradiation with UV light.

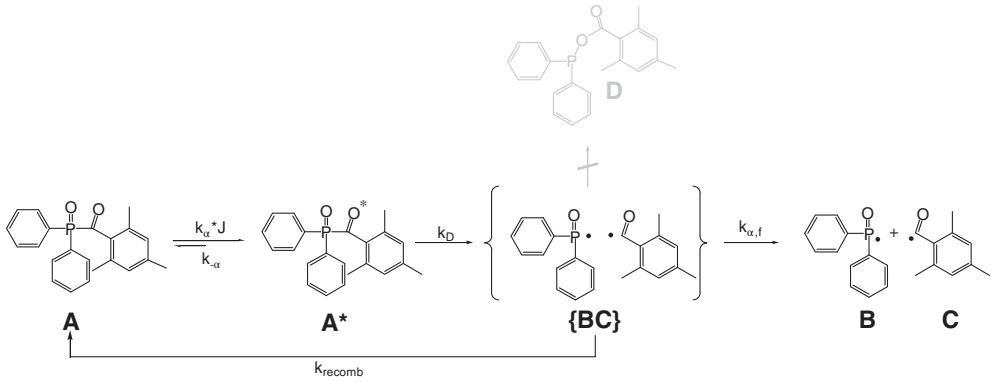

Figure 5. Principle assumed initiation mechanism for TPO.

done using $CDCl_3$ (7.26 ppm in ^1H and ^2H, 77.0 ppm in ^{13}C), d^8-toluene (CH_3: 2.09 ppm in ^1H and ^2H, 20.4 ppm in ^{13}C) or d^3-MA (CH_3: 3.74 ppm in ^1H and ^2H, 50.5 ppm in ^{13}C) as solvent.

RESULTS AND DISCUSSION

Kinetic Model for the Initiation of TPO

For the quantification of the initiation kinetics, we assume the usual mechanism, applied in principle also for the thermal initiation except for the participation of UV-light (Figure 5; TPO as example). On irradiation, a photo-excited state **A*** of the initiator is formed (we do not distinguish between singlet and triplet excited state). This photo-excited state can be quenched reforming the initiator **A** or it can further react in the Norrish-Typ I α-cleavage reaction to form two radicals which in first instance remain close to each other (cage compound **{BC}** in Figure 5). These two radicals can recombine in a back-reaction and re-form the initiator **A** or they can further react with the monomer initiating the polymerization.

Compound **{BC}** is in general called solvent-caged radical pair, while the compounds **B** and **C** are referred to as solvent-separated radicals. In our case, we point out that the solvent is identical to the monomer.

On the basis of this reaction scheme for the derivation of the kinetic differential equations, we assume as usual the Bodenstein stationary principle for the compounds **A*** and **{BC}**. Additionally, a first-order dependence in all contributing compound concentrations including the light intensity was used for the description. The latter assumption was proven to be valid for compound **A** and for the light intensity by means of concentration dependent, respectively light intensity-dependent, measurements as will be shown below. On this basis, the following eqs. (1)–(3) can be derived for the initiation kinetics of TPO (for the detailed derivation, see Supporting Information Figure S52).

$$\text{Quantum yield}: Q_\alpha = \frac{k_D}{k_{-\alpha} + k_D} \tag{1}$$

$$\text{Initiator efficiency}: E_\alpha = \frac{k_{\alpha,f}}{k_{\text{recomb}} + k_{a,f}} \tag{2}$$

$$-\frac{dc_A(t)}{dt} = \frac{dc_B(t)}{dt} = \frac{dc_C(t)}{dt} = E_\alpha \cdot Q_\alpha \cdot k_\alpha \cdot J(t) \cdot c_A(t) = k'_\alpha \cdot J(t) \cdot c_A(t) \tag{3}$$

Using our evaluation protocol, we will only provide values for $k'_\alpha = k_\alpha \cdot E_\alpha \cdot Q_\alpha$. We cannot extract individual values for the quantum yield Q_α or for the initiator efficiency E_α. The quantum yield of TPO in acetonitrile solution has been determined by others before to 0.56[23] and in dichloromethane solution to 0.4.[24] For the initiator efficiency, we expect values near to 1 because our examination is done in bulk monomer without solvent cage.

Recombination has been reported before to lead to some extend to polymerization-inactive phosphites (**D** in Figure 5) in acetonitrile, which are lost for the initiation reaction.[19] We point out that in our case with the monomer being the solvent we could not observe this side reaction to a significant amount. Exactly two active radicals are formed from TPO and four from BAPO with no significant loss of initiator in any side reaction as proven by TEMPO titration (see below). Also, in *in situ* NMR experiments in deuterated methyl acrylate, we could not detect the phosphite **D** (neither other **B—B** or **C—C** recombination products) in significant amounts (see below).

The main difficulty concerning the evaluation of eq. (3) is that the light intensity because of the Lambert–Beer law becomes concentration- and, thus, time dependent [eq. (4)].

$$J(t) = J_{\max} \cdot e^{-c_A(t) \cdot \varepsilon_{365} \cdot d} \tag{4}$$

In eq. (4) $J_{\max}$ is the intensity of the LED device, c_A is the concentration of initiator, ε_{365} is the extinction coefficient of the initiator at 365 nm, and d is the thickness of the sample.

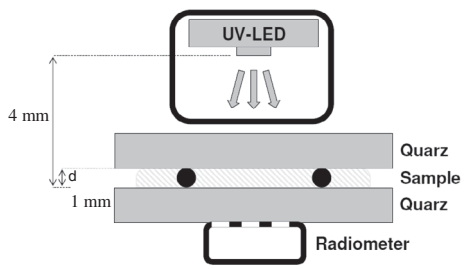

Figure 6. Schematic set-up for the radiometer measurements. The black cycles represent glass fibers of defined thickness (also see the Supporting Information Figure S49).

The consequence is that eq. (3) cannot be solved analytically, and the data evaluation must be done by simultaneous numerical solution of eqs. (3) and (4). We used the numerical solver program POLYMATH for our evaluation (for program codes, see Supporting Information Figures S55–S58).

The data collection of the initiation kinetics was performed in acrylate monomer solution by means of two independent methods to double-check our results. First, we used the time-dependent absorption behavior of samples with defined thickness measured by means of a radiometer (initiator decay with time), and second, we trapped the formed radicals with defined amounts of TEMPO monitoring the presence or the absence of polymerization at defined thicknesses and after defined irradiation times by means of ATR FTIR spectroscopy (TEMPO titration; radical formation with time; the validity of this method will be proven below). According to eq. (3), both methods should lead to the same kinetic parameters providing an intrinsic double check of the results.

Evaluation of the Initiator Decay by Means of the Time-Dependent Light Absorption Behavior of Initiator/EHA Mixtures Measured via Radiometer

For the initiator decay experiments defined mixtures of the initiator in 2-ethyl hexyl acrylate (EHA) were prepared (0.25—2 mol %) and placed between two quartz plates to exclude air from the sample surface which were separated by two glass fibers of defined diameter to provide defined thicknesses (50 µm, 120 µm, 200 µm, each ±7 µm) of the samples (Figure 6).

The quartz plates were checked separately without sample to absorb less than 1% of light intensity of the irradiation source. Air dissolved in the sample volume was proven not to influence the initiation behavior by comparing the results of degassed solutions with those that were not degassed prior to usage, and no differences were observed. The inhibitor present in commercial EHA was removed as described in the experimental section.

The POLYMATH program code used for the numerical evaluation is documented in the Supporting Information (Figure S55: "CODE_TPO_RADIO"). The program code requires initial values for ε_{365} and k_α' which are not known in the first place. These values can be very confidently be determined by a simplified evaluation, assuming an averaged time-independent light intensity [eq. (5)], where τ is the irradiation time, J_{max} is the intensity of the light source, ε_{365} is the extinction coefficient of the initiator at 365 nm, d is the thickness of the sample, and c_A^0 is the initiator starting concentration.

$$\hat{J} = \frac{1}{2}\cdot[J(\tau)+J(0)] = \frac{1}{2}\cdot\left[J(\tau)+J_{max}\cdot e^{-c_A^0\cdot\varepsilon_{365}\cdot d}\right] \quad (5)$$

$$\ln\left[\ln\left(\frac{J_{max}}{J(\tau)}\right)\right] = \ln\left(c_A^0\cdot\varepsilon_{365}\cdot d\right) - k'_\alpha\cdot\hat{J}\cdot\tau \quad (6)$$

The application of eq. (5) to eq. (3) allows for an analytical solution of eq. (3), which results in eq. (6) (for derivation, see Supporting Information Figure S53). Equation (6) exclusively contains experimentally available data and can be evaluated by means of linear regression, when $\ln[\ln(J_{max}/J(\tau))]$ is plotted versus $\hat{J}\cdot\tau$. From the slope of this plot, k'_α can be extracted. From the intersection with the y axis, ε_{365} is received. A first value for $J(0)$ must be settled by using the result for the light intensity of the smallest τ (20 ms in our case). On the basis of this approximation, the values for ε_{365} and k'_α can be optimized by adjusting ε_{365} to bring eqs. (5) and (6) to self-consistence with the same ε_{365} value.

Figure 7 shows an exemplary plot for the application of eq. (6) on the experimental results (for all series of these plots, see Supporting Information Figures S59–S67). Table I contains the extracted data evaluated for different initiator starting concentrations and sample thicknesses.

Figure 8 shows exemplarily the very satisfactory description of the experimental data by the data calculated from the POLYMATH program using the averaged values for ε_{365} and k'_α of Table I proving the justification of our assumptions concerning the first order in all participating components (see also Supporting Information Figure S68 for concentration-dependent graph at 120 µm).

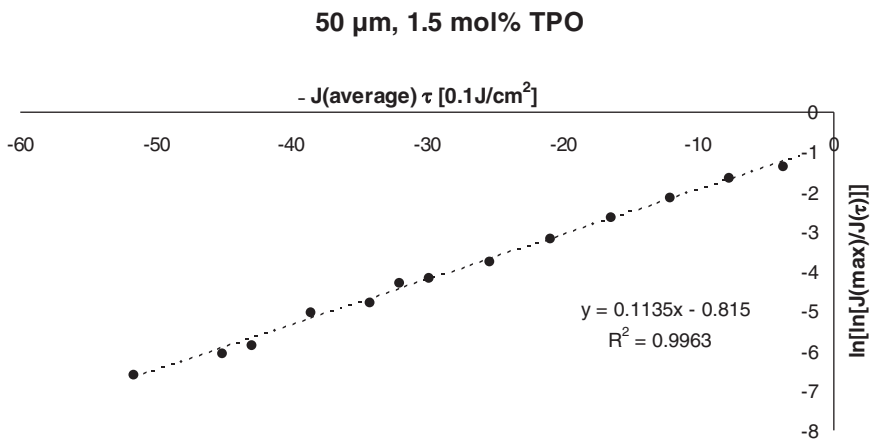

Figure 7. Application of eq. (6) on the radiometer results concerning the initiator decay (sample thickness: 50 µm, initiator starting concentration: 1.5 mol %).

Table I. Data Extracted From the Evaluation of eq. (6)

Concentration (mol %)	Sample thickness (μm)	ε_{365} 10^3·(mol%$^{-1}$·μm^{-1})	k'_α 10^6·[(mW cm^{-2})$^{-1}$·ms^{-1}]
1	50	5.7198	8.98
1.5	50	5.9019	11.35
2	50	5.3881	10.64
1	120	5.5665	7.97
1.5	120	5.6877	10.73
2	120	5.3123	9.47
1	200	5.9527	9.74
1.5	200	5.3312	9.63
2[a]	200[a]	4.9125[a]	8.36[a]
Average		5.61 ± 0.32	9.81 ± 1.12

[a] The value for 200 μm/2 mol % was not used for the determination of the average. A reason for the comparatively large deviation concerning ε_{365} under these conditions is given below in this article.

We point out that the experimental radiometric results are independent of whether the irradiation is done in one large irradiation step τ or whether several shorter consecutive irradiation pulses which add together in total to τ are applied, supporting further the reliability of our applied method and results.

Evaluation of Radical Formation Kinetics by Means of TEMPO-Titration of the TPO/EHA Mixtures Measured via ATR FTIR Spectroscopy

As a second independent method to quantify the kinetic parameters of the UV-triggered initiation we chose to use trapping experiments with defined amounts of inhibitor present in the initiator/EHA mixture.

We examined the suitability of three different inhibitors (Figure 9).

The 2,2-diphenyl-pikryl hydrazyl radical (DPPH) as well as the galvanoxyl radical showed too strong self-absorption at 365 nm and could, thus, not be used. TEMPO in contrast was checked to have no significant absorption at 365 nm by means of radiometric measurement.

Still, as our examinations were done in pure liquid acrylate monomer it could not be expected in the first place that stoichiometric amounts of TEMPO are sufficient to prevent the polymerization, and, thus, we further had to critically examine this strategy and prove its reliability. TEMPO as trapping reagent has been used before (applied in excess and not stoichiometrically) in context with acyl phosphine oxides to elucidate the initiation mechanism.[19,20]

To prove the validity of the TEMPO titration approach, we collected two additional pieces of information. First, we examined the minimum amount of TEMPO necessary to prevent the polymerization, even after having completely activated the initiator. We found that for TPO we reached this target with exactly two equivalents of TEMPO and for BAPO with four equivalents of TEMPO in accordance with the expectation of a stoichiometric inhibition brought about by TEMPO (see Supporting Information Figures S70 and S71).

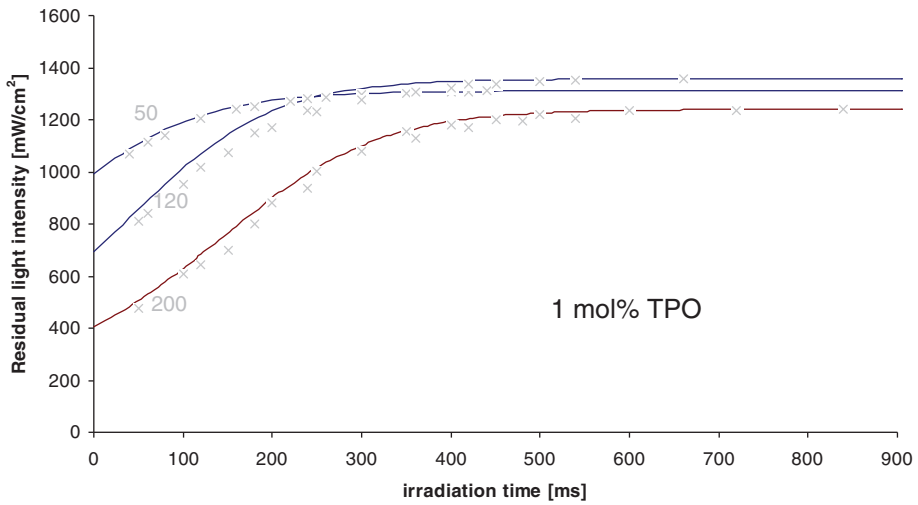

Figure 8. Comparison of experimental (cross) and calculated (line) data for the initiator decay at 25°C with 1 mol % of TPO with three different thicknesses (50, 120, 200 μm). [Color figure can be viewed at wileyonlinelibrary.com]

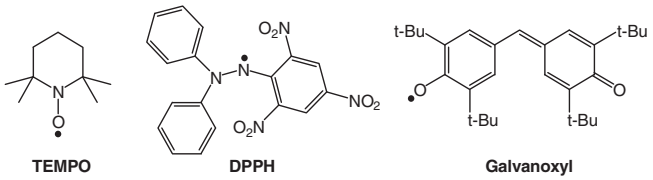

Figure 9. The three inhibitors that were tested within this study. Only TEMPO was useful as discussed in the text.

Second, we performed NMR studies to gain knowledge about the reactions taking place during the inhibition. The NMR studies were done in methyl acrylate that was triply deuterated at the methyl group (d^3-MA) to enable locking while performing the NMR measurement. The deuteration at the methyl group was expected to be far enough from the reaction center to avoid any kind of disturbing isotopic effect. As initiators, TPO and ^{13}C-TPO (TPO with a ^{13}C-labelling at the carbonyl carbon) were applied. The ^{13}C-labeling at the carbonyl carbon was necessary to unequivocally follow the fate of the mesityl carbonyl fragment of the initiator during the initiation process by means of ^{13}C NMR spectroscopy.

The reaction of ^{13}C-TPO with two equivalents of TEMPO in toluene-d^8 on irradiation with the 365 nm-LED quantitatively leads to the two expected reaction products (Figure 10).

In ^{31}P NMR spectroscopy the doublet of ^{13}C-TPO at 15 ppm vanishes completely in favor of a singlet at 31 ppm for DPO_TEMPO. In ^{13}C NMR spectroscopy, the doublet of ^{13}C-TPO at 220 ppm vanishes completely in favor of a singlet at 168 ppm for Mes^{13}CO_TEMPO (Figure 11). The two products can be separated by acetonitrile/hexane extraction. The acetonitrile fraction contains mainly DPO_TEMPO which can further be purified by washing with hexane and be isolated as white powder. After drying the hexane phase of the acetonitrile/hexane extraction, a white solid was received which on additional extraction with hexane results in quite pure Mes^{13}CO_TEMPO as a white powder (Supporting Information Figures S28–S36).

If a 1 mol % solution of ^{13}C-TPO or TPO in d^3-MA without TEMPO is irradiated with short-light pulses, the polymerization can be monitored by means of ^{31}P and ^{13}C NMR spectroscopy (Figure 12). As can be seen from these measurements, the DPO end group bound to a PMA chain shows a signal in ^{31}P NMR spectroscopy at about 27.5 ppm (no peaks for the phosphite **D** were detected, expected at about 100 ppm and 30 ppm as doublets), while the Mes^{13}CO end group bound to a PMA chain causes a signal in ^{13}C NMR spectroscopy at about 207 ppm.

The irradiation of a 1 mol % solution of ^{13}C-TPO or TPO in d^3-MA containing two equivalents of TEMPO was analogously examined by means of ^{31}P and ^{13}C NMR spectroscopy (Figure 13).

As can be seen, the MesCO radical is quenched quantitatively by forming MesCO_TEMPO (the only peak in the ^{13}C NMR spectrum at 174 ppm). The DPO-radical forms two products, one of them being DPO_TEMPO as indicated by the peak at 31 ppm in the ^{31}P NMR spectrum. A second peak is detected at 24 ppm. These two peaks add together to more than 98% of the intensity in the ^{31}P NMR spectrum. If TEMPO is added in a little lower amount than two equivalents a third small peak is visible at 18 ppm. We were not able to assign this small peak (it is not diphenyl phosphine oxide as proven by measuring without ^{1}H decoupling; the peak remained a singlet). However, we were able to isolate the compound responsible for the peak at 24 ppm by drying the sample and washing the residual white solid with several portions of hexane. The NMR and IR spectroscopic data are in accordance with a molecule in which one MA has been initiated by the DPO-radical followed by a trapping through TEMPO (Supporting Information Figures S24–S27).

This quite low amount of reacted monomer will not disturb the results of the TEMPO titration, because the range of measurement error with about 5% is larger. The NMR results prove that the TEMPO titration is valid for the evaluation of the photoinitiation kinetics in this system. However, it still remained obscure in our eyes why in the bulk monomer TEMPO is such an efficient inhibitor. Our most convincing chemical explanation was that there might be a Lewis acid/base interaction between TEMPO and either the phosphorus atom or the carbonyl carbon atom of TPO or both, keeping the inhibitor in close proximity to the initiator. To find experimental evidence for this proposal, we performed NMR and IR measurements of TPO (^{13}C-TPO for the NMR measurement) in toluene, increasing stepwise the amount of TEMPO added to the solution (we note that ESR devices were not accessible for us; ESR studies on TPO irradiation in benzene were published before[21]). By these experiments, we wanted to check whether a contact shift is detectable in the ^{13}C NMR spectrum for the carbonyl carbon atom or in ^{31}P NMR spectrum for the phosphorus atom. In the IR measurement a shift of the wave number for the ν(C═O) stretching vibration at 1665 cm^{-1} or the ν(P═O) stretching vibration at about 1210 cm^{-1} in TPO, dissolved in toluene without TEMPO, would have been a probe for the proposed interaction, if found on addition of TEMPO to this solution.

Figure 14 illustrates how the chemical shift of the ^{13}CO peak and the one for the ^{31}P peak of ^{13}C-TPO develop with increasing amount if TEMPO. For the ^{31}P signal, a linear increase in the

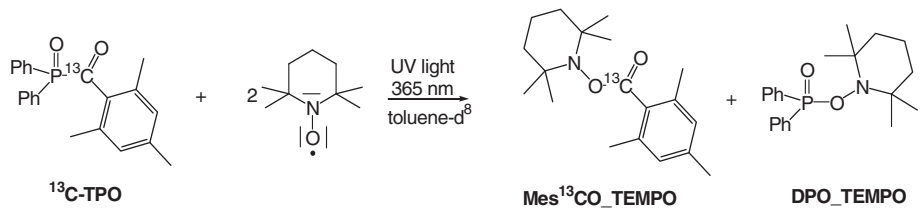

Figure 10. Reaction of ^{13}C-TPO with two equivalents of TEMPO in toluene-d^8 on irradiation with UV-light.

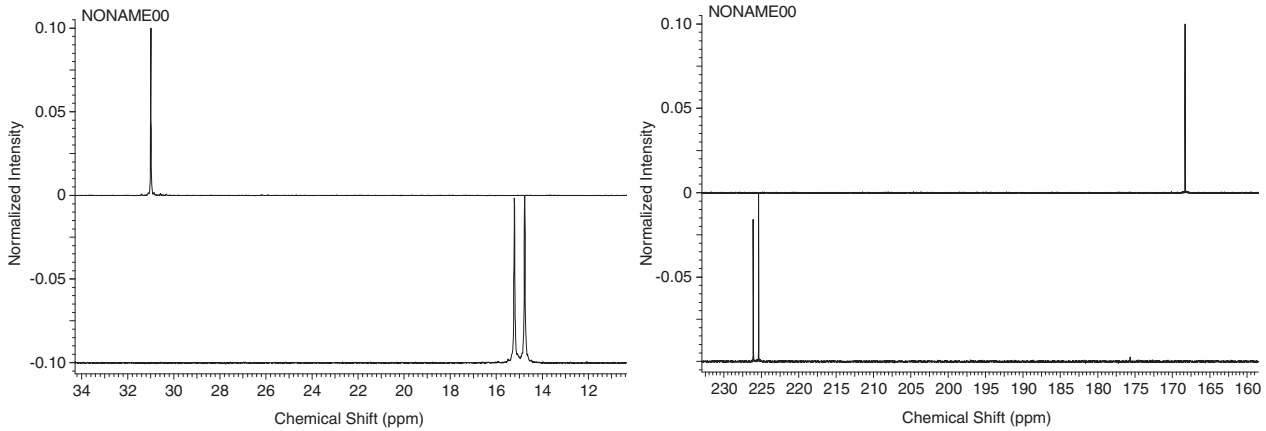

Figure 11. Excerpts of the ^{31}P NMR spectrum (left) and ^{13}C NMR spectrum before irradiation (bottom) and after complete conversion on irradiation (top) of the reaction shown in Figure 10.

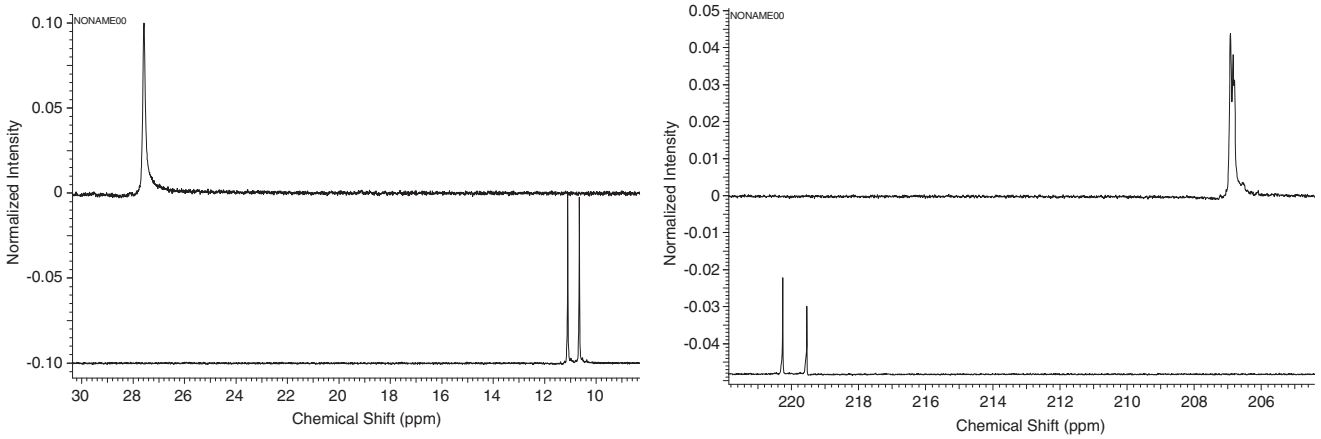

Figure 12. UV-light initiated bulk polymerization of d^3-MA with ^{13}C-TPO (1 mol%) monitored by means of ^{31}P NMR (left) and ^{13}C NMR (right) spectroscopy (bottom: start; top: end).

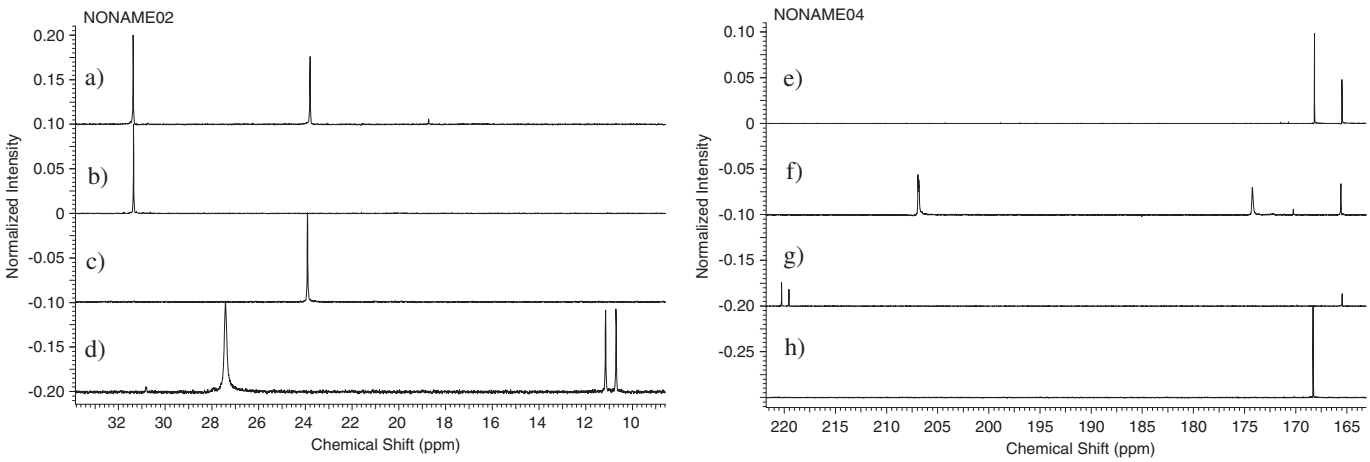

Figure 13. Final ^{31}P (left) and ^{13}C (right) NMR spectra for the irradiation of ^{13}C-TPO in d^3-MA in the presence of two equivalents of TEMPO. (a) ^{31}P NMR spectrum for ^{13}C-TPO plus 2 eq TEMPO (irradiated in d^3-MA). (b) ^{31}P NMR spectrum of isolated DPO-TEMPO. (c) ^{31}P NMR spectrum of isolated DPO_MA_TEMPO. (d) ^{31}P NMR spectrum for ^{13}C-TPO (irradiated in d^3-MA). (e) ^{13}C NMR spectrum for ^{13}C-TPO plus 2 eq TEMPO (irradiated in d^3-MA). (f) ^{13}C NMR spectrum for ^{13}C-TPO (irradiated in d^3-MA). (g) ^{13}C NMR spectrum for ^{13}C-TPO (non-irradiated in d^3-MA). (h) ^{13}C NMR spectrum of isolated MES^{13}CO_TEMPO. The results prove that no polymerization occurs under these conditions. Partly one molecule of d^3-MA is inserted. However, a titration of the reaction with TEMPO is accurate.

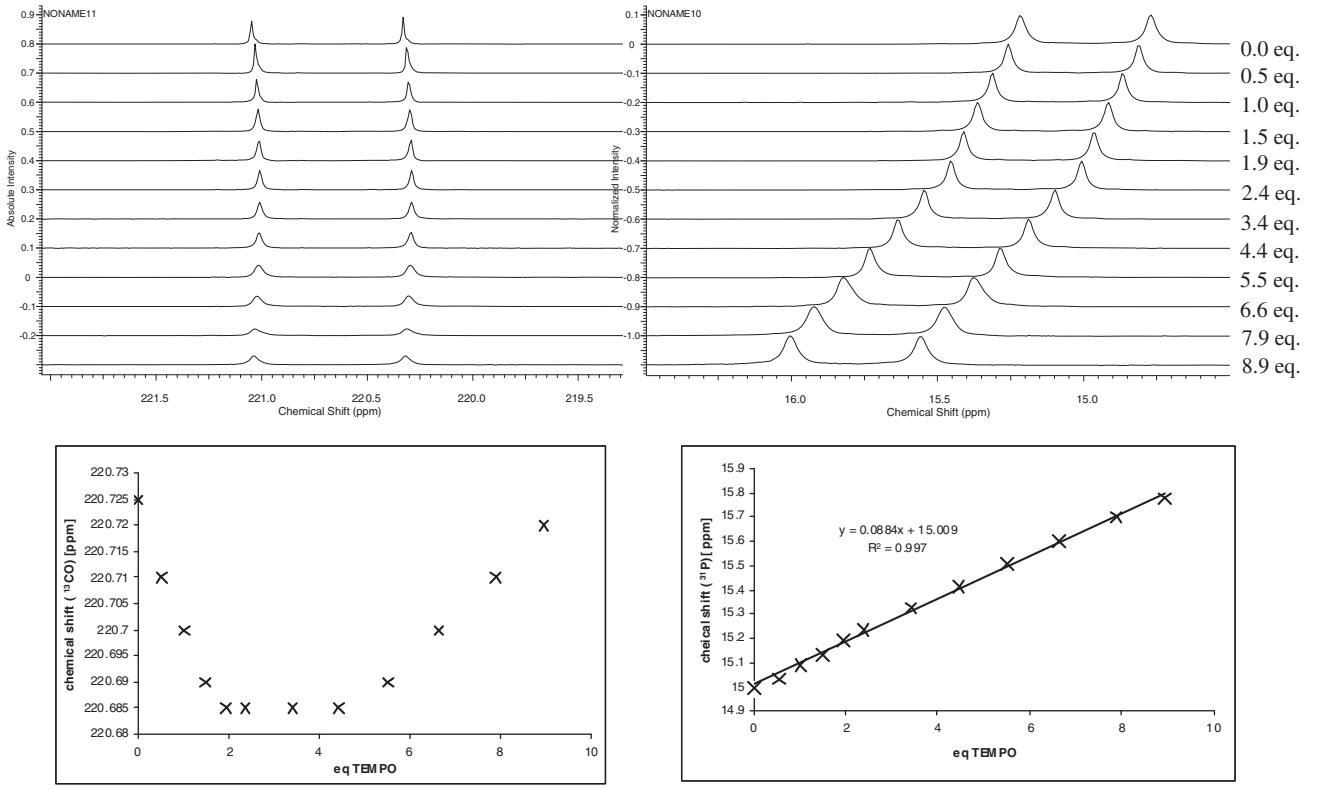

Figure 14. Contact shifts for the ^{13}CO peak (left) and the ^{31}P peak (right) of ^{13}C-TPO with increasing amount of TEMPO present in 1 mol % d^8-toluene solution.

chemical shift is found which is indicative for a nonspecific interaction between ^{13}C-TPO and TEMPO in general related to simple collisions between the two molecules.[27] A similar linear increase of the chemical shift is also found for the toluene-d^8 signals in ^{13}C NMR spectroscopy (see Supporting Information Figures S37–S43). However, for the ^{13}CO signal unequivocally a shift to lower ppm is found up to about 2 eq of TEMPO. Only, at higher amounts of TEMPO the nonspecific collision interaction between ^{13}C-TPO and TEMPO becomes dominant.

We propose that this can be taken as an evidence for a weak donor/acceptor interaction between the carbonyl carbon of TPO and TEMPO, while a similar kind of interaction between the phosphorus atom of TPO and TEMPO cannot be supported. Similar conclusions about hydrogen bonding interactions involving TEMPO have been drawn before, and Lewis acid/base adducts containing TEMPO are known in principle.[28–34]

IR measurements of TPO in toluene with increasing amount of TEMPO showed that for the ν(C═O) stretching vibration the wave number increases slightly but systematically from 1664.7 cm^{-1} without TEMPO to 1666.3 cm^{-1} in the presence of nine equivalents of TEMPO to higher values (Supporting Information Figures S42–43). We note that this is a quite small change. In case of hydrogen bondings, for example, wave numbers for ν(C═O) stretching vibrations are shifted to lower values by about 20–40 cm^{-1}. The shift to higher wave numbers in our case might be explained by a less efficient conjugation of the CO group with the aromatic mesityl ring if TEMPO interacts with the carbonyl carbon. While the peak at 1665 cm^{-1} can unambiguously be related to the ν(C═O) stretching vibration by comparison of the IR spectra of TPO and ^{13}C-TPO (Supporting Information Figures S33–S34), the situation is more ambiguous for the ν(P═O) stretching vibration. In the expected range of 1200–1300 cm^{-1}, two peaks are found for TPO in toluene solution. The wave numbers of both of them decrease slightly but systematically with increasing amount of TEMPO present. Although this decrease in the wave number of the ν(P═O) stretching vibration would be in accordance with a donor acceptor interaction between the TPO phosphorus atom and TEMPO, the ambiguity about the peaks and the too small changes [for ν(C═O) as well as for ν(P=O)] do not allow to unequivocally support this kind of interaction on the basis of the IR results alone.

As a conclusion of the NMR and IR results of TPO in toluene with varying amount if TEMPO present, we propose that a donor/acceptor interaction can be justified for the carbonyl carbon of TPO. For the phosphorous atom this kind of interaction remains at least under question. In any case this interaction (if present) is quite weak for both atomic centers, and still in time average it would force the TEMPO in close proximity to the TPO molecule, which according to our proposal, is the main secret for the fact that the TEMPO titration works so confidently. Figure 15 summarizes our proposal concerning the inhibiting mechanism of TEMPO with TPO. Three products are formed. Two of them are the direct recombination products between the fragments of the UV-light induced homolytic cleavage of TPO and TEMPO. The third one is the product of recombination between the DPO radical, having added one acrylate molecule, and TEMPO. Thus,

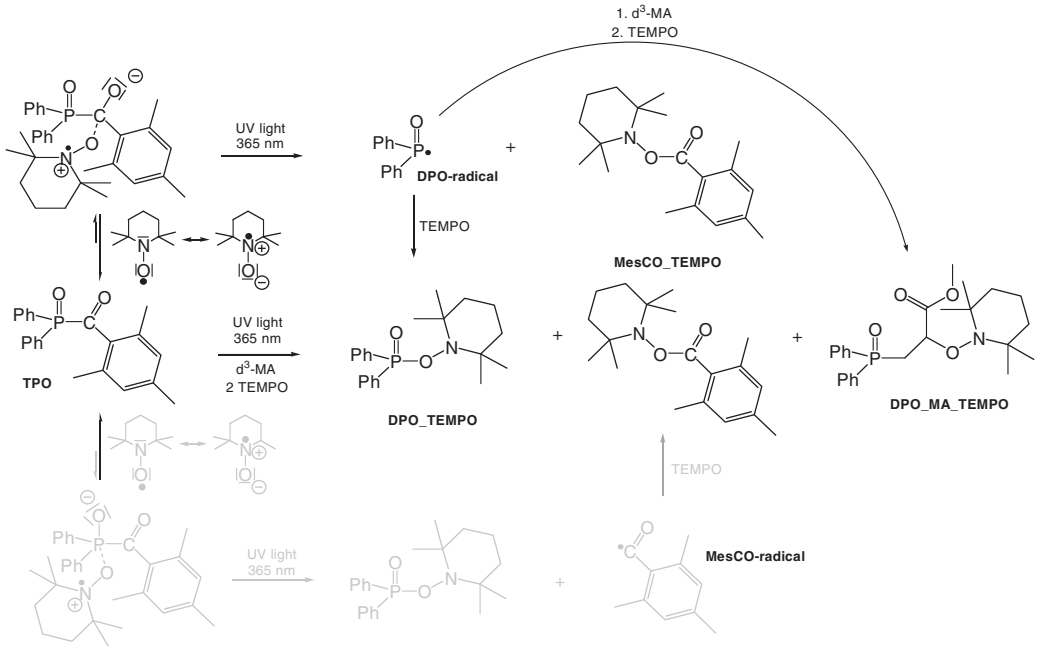

Figure 15. Proposed mechanism of the inhibition of TPO by reaction of TEMPO in neat acrylate monomer.

unequivocally TEMPO can be used in a stoichiometric titration to determine the number of formed radicals. Because of the proposed donor/acceptor interaction the TEMPO is in average in close proximity to the TPO molecule and immediately traps any radical, formed by UV-light irradiation prior to a reaction with the acrylate monomer. Two reasons can be named for the finding that only from the DPO radical a monomer can be initiated before the trapping with TEMPO, but not from the MesCO-radical. First, it is known from earlier publications that the phosphinoyl radical is decisively more reactive than the benzoyl radical.[23] And secondly, according to our NMR results, the donor/acceptor interaction is more pronounced for the carbonyl carbon as compared to the phosphorous atom, keeping the TEMPO molecule in average nearer to the carbonyl carbon center as compared to the phosphorous atom.

The TEMPO titration was performed using the set-up depicted in Figure 16 (see also Supporting Information Figure S49). Defined molar concentrations of initiator in EHA solution were prepared containing defined amounts of TEMPO. A drop of this solution was placed on the ATR sensor. Two glass fibers with defined thickness were added aside to the sensor as spaceholders. The same quartz glass used also for the radiometric measurements (less than 1% absorption of the irradiated light) was placed on top to guarantee a defined thickness and to avoid contact to air. A defined light pulse was applied to the sample, followed by FTIR measurement to determine changes [because of the highest sensitivity the peak for the ν(C—O) vibration at 1190 cm^{-1} was used; Figure 17]. If no polymerization was detected a second pulse was applied. Since the ATR technique is surface sensitive and only penetrates into the sample by about 6–10 µm, the IR spectra show changes brought about by irradiation at a thickness adjusted by the diameter of the glass fibers. Thus, on finding the amount of TEMPO which leads to no polymerization at the thickness d on irradiation with pulse length τ, the amount of radicals formed at this thickness d in the time τ can be quantified directly.

The more the added TEMPO amount is lower than the critical amount to prevent polymerization, the more pronounced will be the polymerization step brought about by the noninhibited radicals of the initiator. If more TEMPO is added than the necessary critical amount the size of the step on applying a second light pulse tells how far away from the critical amount the access is (see the Supporting Information Figures S69–S70).

Thus, finding the cutting point between detecting the polymerization on the first irradiation pulse and not detecting a significant polymerization on the second irradiation pulse allows confidently for determining the amount of formed radicals at a defined thickness and irradiation time. Figure 18 shows exemplarily the results of these

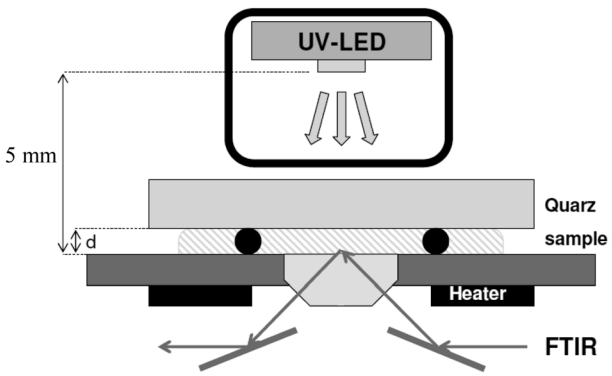

Figure 16. Set-up for the UV-light irradiation on the ATR-FTIR device used for the TEMPO titration (see also the Supporting Information Figure S49).

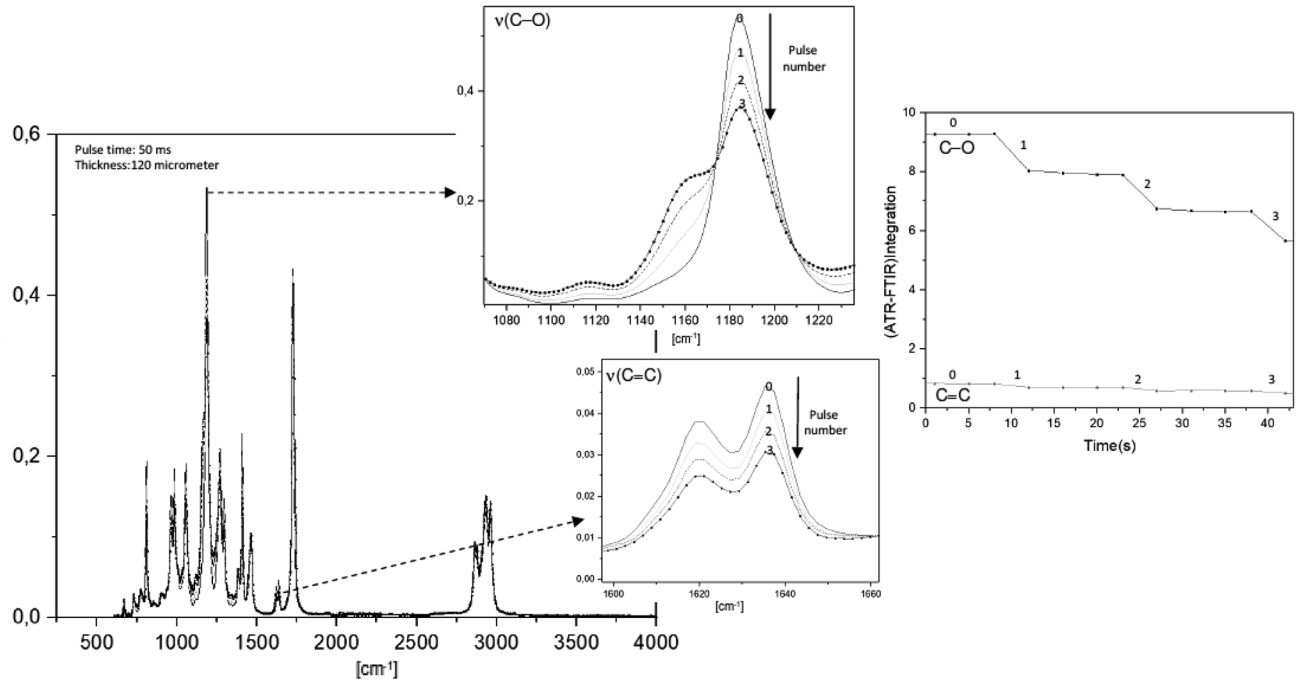

Figure 17. Representative IR picture with steps.

experiments with TPO (see also Supporting Information Figure S71). In this figure, the calculated values are also labeled using the averaged kinetic parameters from the radiometric measurements in Table I. They were calculated using POLYMATH (for program code, see Supporting Information "CODE_TPO_TEMPO"). As can be seen both independent methods lead to very close experimental results, emphasizing the reliability of the methods and the extracted data.

Kinetic Model and Evaluation for the Initiation of BAPO

The very successful evaluation protocol for the initiation kinetics of TPO was transferred to the related but more complex case of BAPO. Figure 19 shows the principle initiation mechanism assumed for BAPO, which contains two steps and can create in total four polymerization active radicals. Indeed in both our radiometric measurements as well as the TEMPO titration experiments (see Supporting Information Figures S74–S75), we could prove that exactly four equivalents of TEMPO are necessary to completely suppress any polymerization even after elongated irradiation time and complete initiator decay.

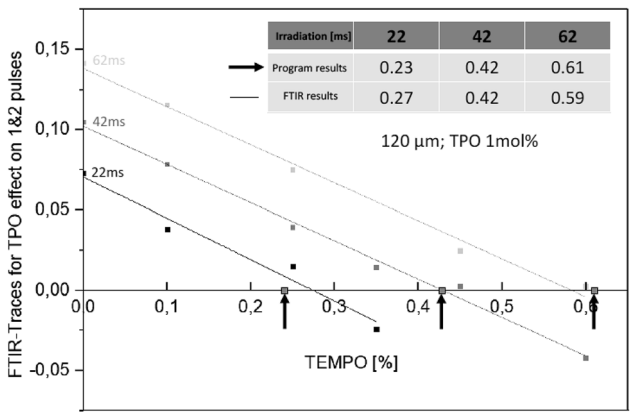

Figure 18. Results of the TEMPO titration experiments with TPO, T: 25 °C, d: 120 µm, c_A^0 = 1 mol %.

For the quantification of the initiation kinetics, we assumed that the two α cleavages in BAPO are considered kinetically identical (same rate constant k_α, same initiator efficiency E_α, same quantum yield Q_α for **A′** and **B′**; this is our most critical assumption, justified by the final very good fitting results on applying it; see below) and independent of each other (Figure 19). These assumptions lead to the kinetic differential equations eqs. (7)–(9).

$$\frac{dc_{A'}(t)}{dt} = -k'_\alpha \cdot J(t) \cdot c_{A'}(t) \tag{7}$$

$$\frac{dc_{B'}(t)}{dt} = k'_\alpha \cdot J(t) \cdot c_{A'}(t) - k'_\alpha \cdot J(t) \cdot c_{B'}(t) = k'_\alpha \cdot J(t) \cdot [c_{A'}(t) - c_{B'}(t)] \tag{8}$$

$$\frac{dc_C(t)}{dt} = k'_\alpha \cdot J(t) \cdot c_{A'}(t) + k'_\alpha \cdot J(t) \cdot c_{B'}(t) = k'_\alpha \cdot J(t) \cdot [c_{A'}(t) + c_{B'}(t)] \tag{9}$$

On this basis again the simplification of eq. (5) was applied for the evaluation of the experimental results of the initiator decay by means of radiometric measurement, which in turn leads to eqs. (10)–(12), where as a first approximation an averaged extinction coefficient identical for A′ and B′ was assumed additionally (for a detailed derivation see the Supporting Information Figure S54).

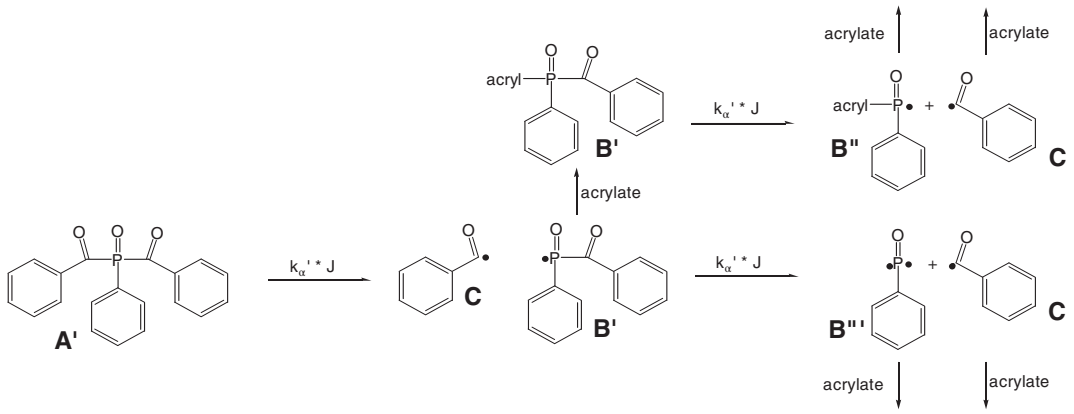

Figure 19. Initiation mechanism for BAPO showing the assumed identical behavior of compounds **A′** and **B′**.

$$J(\tau) = J_{\max} \cdot e^{-[c_{A\prime}(\tau) + c_{B\prime}(\tau)] \cdot \hat{\varepsilon}_{365} d} \tag{10}$$

$$\hat{J} = \frac{1}{2} \cdot (J(\tau) + J(0)) = \frac{1}{2} \cdot \left(J(\tau) + J_{\max} \cdot e^{-c^0_{A\prime} \cdot \hat{\varepsilon}_{365} \cdot d} \right) \tag{11}$$

$$\ln\left[\ln\left[\frac{J_{\max}}{J(\tau)}\right]\right] = \ln\left[c^0_{A'} \cdot \hat{\varepsilon}_{365} \cdot d\right] + \ln\left[1 + k'_\alpha \cdot \hat{J} \cdot \tau\right] - k'_\alpha \cdot \hat{J} \cdot \tau \tag{12}$$

Thus, a linear regression on plotting $\ln[\ln[J_{max}/J(\tau)]]$ versus $[\ln(1 + k'_\alpha \cdot \hat{J} \cdot \tau) - k'_\alpha \cdot \hat{J} \cdot \tau]$, for which a slope of 1 is expected, will allow for evaluating the averaged extinction coefficient $\hat{e}_{365}$. In order to be able to do this evaluation, an assumption must be made concerning the rate constant k'_α. We first just transferred the value determined for TPO on this purpose taking into account that the reactivity of the radicals formed from TPO and from BAPO should be comparable. Although a linear correlation according to eq. (12) was found on this assumption, the slope of it decisively deviated from the expected value of 1 (see Supporting Information Figure S76). As consequence in a next step, we iteratively optimized k'_α in order to reach a slope as close as possible to 1 (Figure 20).

The averaged extinction coefficient $\hat{e}_{365}$ ($7.69 \pm 0.87 \cdot 10^{-3}$ mol %$^{-1}$·µm^{-1}) and the k'_α [$11.69 \pm 2.09 \cdot 10^{-6}$ (mW cm^{-2})$^{-1}$·ms^{-1}] values received from this evaluation fitted the experimental data well for long irradiation times. However, decisive deviations were found for short ones for which the averaged $\hat{e}_{365}$ was too small (Figure 21).

We concluded from this finding that individual extinction coefficients $\varepsilon^{A'}_{365}$ and $\varepsilon^{B'}_{365}$ for the compounds **A′** and **B′** must be taken into account where $\varepsilon^{A'}_{365} \approx 2\ \varepsilon^{B'}_{365}$ (since **A′** contains two chromophoric benzoyl groups while **B′** only one) and $\hat{e}_{365} \approx ½ (\varepsilon^{A'}_{365} + \varepsilon^{B'}_{365})$. Taking the equation marks for real leads to a decisive improvement in the description and prediction of the experimental data (Figure 21). A further optimization considering these relations as approximations and using POLYMATH (for the program code, see the Supporting Information Figure S57 "CODE_BAPO_RADIO") led to our final fitting parameters for BAPO: $11.69 \pm 2.09 \cdot 10^{-6}$ (mW cm^{-2})$^{-1}$·ms^{-1}; $\varepsilon^{A'}_{365} = 12.7 \pm 1.43 \cdot 10^{-3}$ mol %$^{-1}$·µm^{-1}, $\varepsilon^{B'}_{365} = 4.0 \pm 0.45 \cdot 10^{-3}$ mol %$^{-1}$·µm^{-1}.

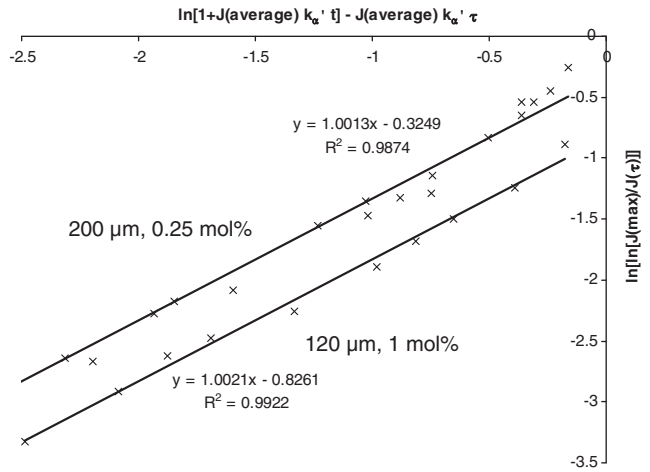

Figure 20. Evaluation for BAPO in EHA according to eq. (12) with optimized value for k'_α.

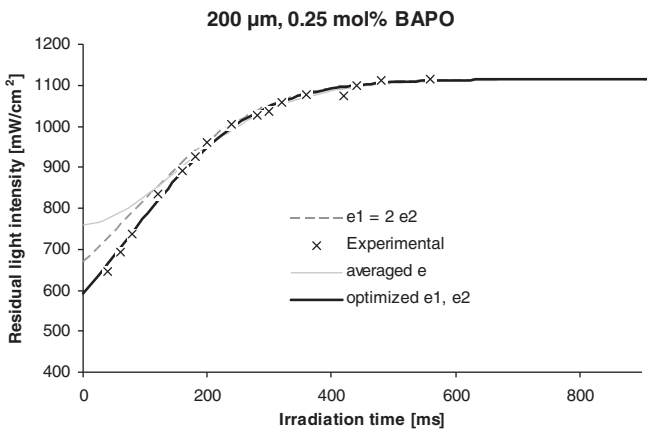

Figure 21. Comparison of experimental radiometric results and fitting results using different parameters sets as described in the text.

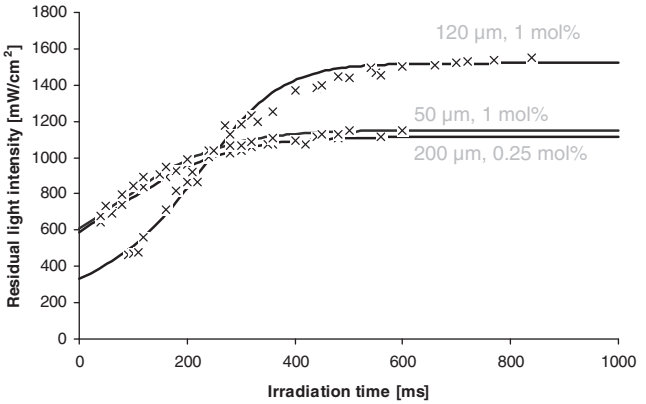

Figure 22. Comparison of experimental (gray) and calculated (black) data for the initiator decay at 25 °C with BAPO.

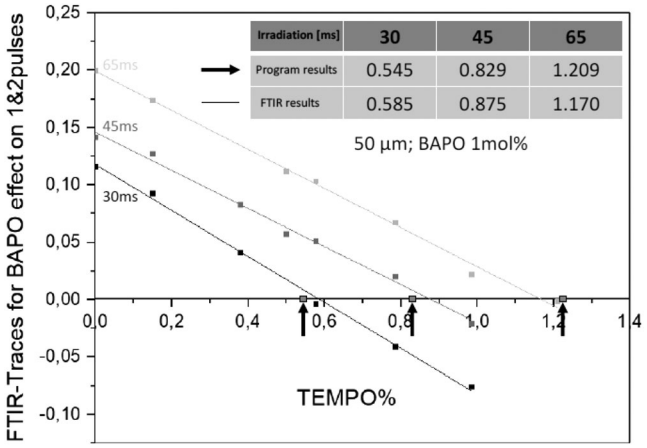

Figure 23. Results of the TEMPO titration experiments with BAPO, *T*: 25 °C, *d*: 50 µm, c_A^0 = 1 mol %.

Figure 22 demonstrates how well the initiator decay can be predicted with our evaluated kinetic data. Taking into account that almost certainly the rate constants for the two species **A′** and **B′** are not exactly identical the accordance between calculated and measured data reached on the basis of this assumption is quite high.

In this context, we notice that at high thickness (such as ≥200 µm) in connection with high initiator concentration (BAPO ≥1 mol %; TPO ≥2 mol %), significant deviations between our proposed and optimized averaged model were observed for both BAPO and TPO in the radiometric measurements (Table I; see Supporting Information Figures S77–78). We propose that the reason for this is a decisive volume shrinkage of the sample during the curing process under these conditions reducing the real thickness during the measurement significantly (we can calculate the averaged real thickness of the sample using our parameters to be about 185 µm rather than 200 µm; with this corrected averaged thickness, the data can be predicted accurately also in this critical range; Supporting Information Figures S77–78). This conclusion is supported by the finding that the TEMPO titration is in good accordance with the predicted values of our averaged data also for the critical concentration/thickness range (Supporting Information Figure S71 and S73). In the TEMPO titration method only the first and second irradiation pulse is used for the evaluation, which is mainly quenched by TEMPO and, thus due to the inhibition and almost no conversion, chemical shrinkage does not play a decisive role in this method.

Figure 23 proves exemplarily that also for BAPO the TEMPO titration method works very well and produces results in strong accordance with the radiometric measurements (see also Supporting Information Figures S72–S73). The calculated values were determined using POLYMATH with the aforementioned evaluated values (for the program code, see the Supporting Information Figure S58 "CODE_BAPO_TEMPO").

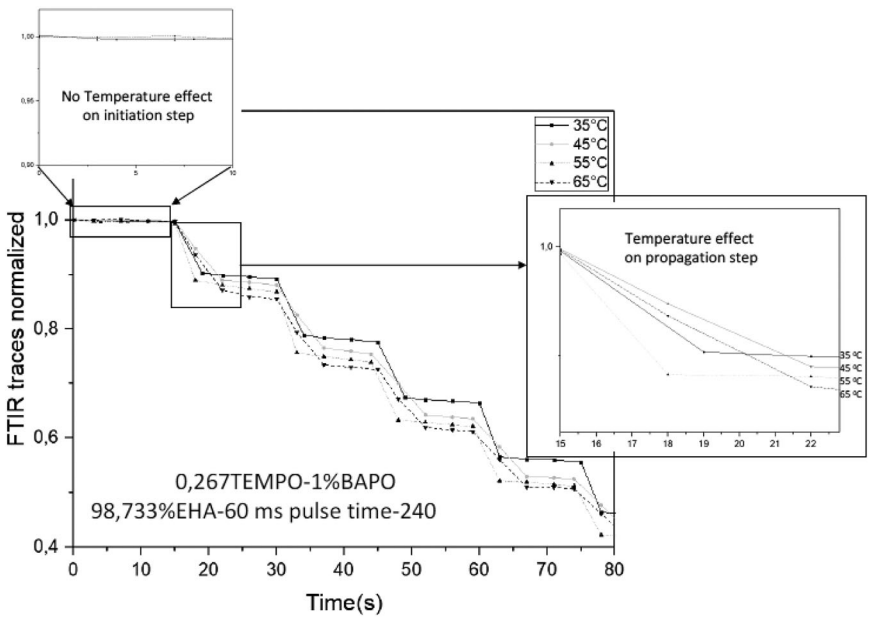

Figure 24. Temperature dependence of the initiation (left, top) and the propagation (right, middle) for BAPO in EHA.

Table II. Thickness Dependence of Dioxygen Quenching on air (BAPO, 1 mol %; Pulse time 60 ms)

Thickness (μm)	Conversion (in air)	Conversion (without air)	Ratio (air/without air)
70	0.12	0.15	0.77
140	0.11	0.11	1
210	0.077	0.077	1
280	0.050	0.050	1

Temperature Dependence

We examined the initiation kinetics of TPO and BAPO in EHA solution in the temperature range between 25 °C and 80 °C to determine the temperature dependence of it by means of adjusting the temperature of the FTIR sensor accordingly (Figure 24).

While on the initiation behavior in the examined temperature range, no influence was found for both tested initiators, the propagation proceeded faster with increasing temperature as expected for a thermal chemical reaction with considerable activation barrier.

An increase in temperature within the thin film caused by the polymerization enthalpy could not be detected with the temperature sensor of the FTIR device. We propose this is because of the large surface/volume ratio of the samples connected with the small dimension in general as well as the contact to the diamond surface on the sensor in the bottom with high thermal conductivity and high heat capacity providing fast heat exchange with the environment (we know, although, by our own experiments that while preparing much thicker and larger specimens for mechanical testing where the surface/volume ratio is small and no contact to a diamond surface is provided, a considerable increase in temperature during the curing process takes place).

Dependence on Air Inhibition

The inhibiting effect of dioxygen in radical polymerizations is well known.[5] Thus, we were interested whether we can quantify the thickness dependence of it for BAPO. On this purpose, we applied adhesive rings of defined thickness (70–280 μm ± 10 μm)

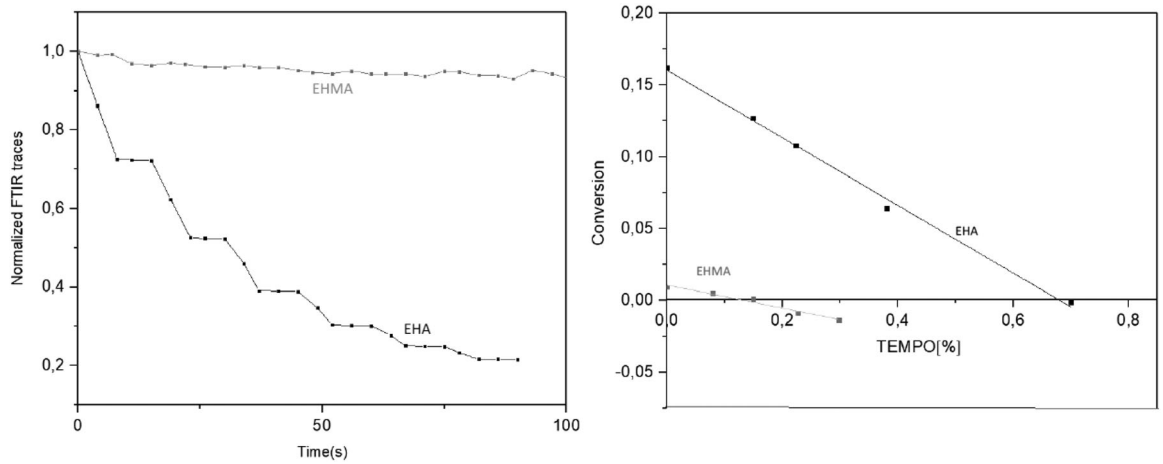

Figure 25. Evidence for an inhibition effect of EHMA on BAPO (1 mol %) during the initiation process (thickness: 50 μm, pulse time: 100 ms).

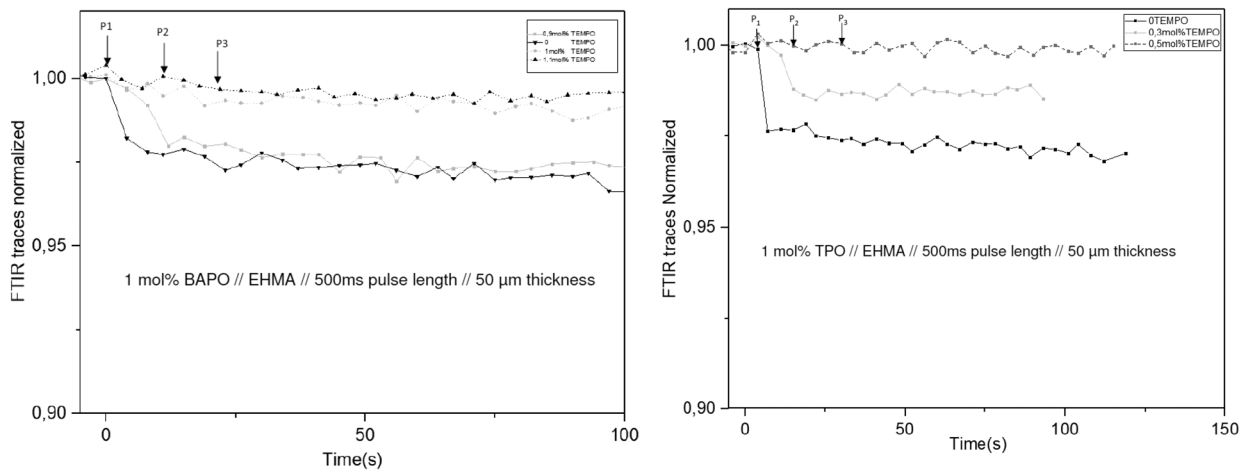

Figure 26. Determination of the total amount of formed polymerization-active radicals in EHMA with BAPO (left) and TPO (right). In both cases, 75% less polymerization-active radicals are formed than expected stoichiometrically (and found for EHA).

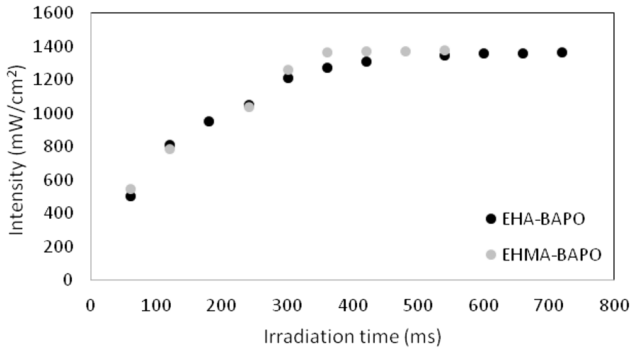

Figure 27. Comparison of BAPO (1 mol %) decay in EHA (black) and EHMA (gray) measured via radiometer as described above (thickness: 120 μm, pulse time: 60 ms).

to our ATR-FTIR device. The center of them served as reservoir which was filled with the BAPO/EHA solution. The top of the sample was, thus, in contact to air while the measurement occurred on the bottom side in a defined distance from the surface.

We point out that these measurements were quite challenging because of the very thin thickness required for these experiments. Still we could show that the influence of dioxygen inhibition becomes significant at distances of about ≤100 μm from the sample surface (Table II). In contrast, no difference was found for deoxygenized monomer solutions and those which were not deoxygenized proving that dissolved traces of dioxygen in the monomer solution do not significantly influence the initiation behavior in our case.

Acrylate/Methacrylate Dependence

In this study, we were interested in whether the change from EHA to ethyl hexyl methacrylate (EHMA) would influence—not only the polymerization rate, from which it is known that methacrylates are decisively slower than acrylates, but also—the initiation behavior of TPO and BAPO. As a consequence, we examined TPO and BAPO in EHMA solution with the same procedure as described previously for EHA. The interesting result was that not only the polymerization rate was slower (smaller slope in Figure 25, right hand side, for EHMA as compared to EHA) but, more importantly, also the amount of formed polymerization-active radicals was decisively smaller (smaller cutting point with the x-axis for EHMA as compared to EHA in Figure 25, right side). Also, the total amount of polymerization-active radicals after complete initiation was decisively lower in case of EHMA as compared to EHA (interestingly for both BAPO and TPO about 75% less polymerization-active radicals in EHMA than expected stoichiometrically and found for EHA; Figure 26).

On the other hand, in our radiometer measurements, the decay of initiator was the same for both initiators in EHA and EHMA (Figure 27).

The conclusion of these results is that EHMA causes an inhibition of the initiators. The origin of it is not yet well understood and will be further examined by us in the future.

CONCLUSIONS

In this article, we have provided a reliable experimental procedure to quantify the initiation kinetics of two important UV-light-triggered initiators for the radical polymerization directly dissolved in the acrylate monomer.

This procedure used two independent methods to double check the evaluated data, the initiator decay via radiometric measurements and the radical formation via TEMPO titration. Both methods result in very close kinetic parameters for TPO and BAPO supporting the reliability of the procedure. A reason for the feasibility of the TEMPO titration was found by means of additional NMR studies using ^{13}C-labeled TPO. Since the benzoyl structure motif is quite common for radical UV-initiators it is likely that the TEMPO titration will also work for other initiators.

On the basis of this procedure, we were able to determine for the first time the necessary kinetic parameters (TPO: $k_\alpha^{'} = 5.61 \pm 0.32 \cdot 10^{-6}$ (mW cm^{-2})$^{-1}$·ms^{-1}, $\varepsilon_{365} = 9.81 \pm 1.12 \cdot 10^{-3}$ mol %$^{-1}$·μm^{-1}\\BAPO: $k_\alpha^{'} = 11.69 \pm 2.09 \cdot 10^{-6}$ (mW cm^{-2})$^{-1}$·ms^{-1}, $\varepsilon_{365}^{A'} = 12.7 \pm 1.43 \cdot 10^{-3}$ mol%$^{-1}$·μm^{-1}, $\varepsilon_{365}^{B'} = 4.0 \pm 0.45 \cdot 10^{-3}$ mol%$^{-1}$·μm^{-1}) for a quantitative prediction of the radical formation with time and thickness for two initiators dissolved in the acrylate monomer. The initiation kinetic parameters proved to be temperatureinvariant while the propagation step showed the expected rate increase with increasing temperature. The importance for dioxygen inhibition from air could be estimated to be relevant in particular at the surface up to a sample thickness of about 100 μm. Concerning the influence of the monomer we found a yet unmentioned inhibiting monomer effect of methacrylates which will further be elucidated in the future by us.

The protocol published in this work can most likely be transferred to other UV-light-triggered initiator precursors in the future and will hopefully help to further increase the availability of quantitative data for UV-triggered initiation systems and, thus, increase the attractiveness of this ultra-fast polyreaction for both academia and industry.

ACKNOWLDGEMENT

Andreas Fischer is acknowledged for the single crystal X-ray diffraction measurement (see Supporting Information).

REFERENCES

1. Sheppard, C. S.; Kamath, V. R. *Polym. Eng.Sci.* **1979**, *19* (9), 597.
2. Akzo Nobel catalogue 2006, Initiators for High Polymers, Code 2161 BTB communication.
3. Brandrup, J.; Immergut, E. H.; Grulke, E. A. Polymer Handbook. 4th ed.; John Wiley: New York, **1999**. p. II/2.
4. Eibel, A.; Fast, D. E.; Gescheidt, G. *Polym. Chem.* **2018**, *9*, 5107.
5. Green, W. A. Industrial Photoinitiators: A Technical Guide; Taylor & Francis: Boca Raton, **2010**.
6. Herold, J.; Kluke, M. *RadTech Report*. **2012**, *3*, 27.
7. Arceneaux, J. A. *RadTech Printer's Guide*. **2016**, 1.
8. Kim, S.; Seo, W. H. *J. Appl. Polym. Sci.* **2004**, *92*, 3921.

9. Glöckner, P.; Jung, T.; Struck, S.; Studer, K. Radiation Curing: Coatings and Printing Inks; Technical Basics, Applications and Trouble Shooting; Vincentz network: Hannover, **2008**.
10. Decker, C. *Prog. Polym. Sci.* **1996**, *21*, 593.
11. Kenning, N. S.; Ficek, B. A.; Hoppe, C. C.; Scranton, A. B. *Polym. Int.* **2008**, *57*, 1134.
12. Böhm, M.; Ruhland, K.; Koch, M.; Spalek, N. *J. Appl. Polym Sci.* **2019**, *136*, 47294.
13. Meereis, C. T. W.; Leal, F. B.; Lima, G. S.; de Carvalho, R. V.; Piva, E.; Ogliari, F. A. *Dent. Mat.* **2014**, *30*, 945.
14. Santini, A.; Torres Gallegos, I.; Felix, C. M. *Prom. Dent. J.* **2013**, *2*(4), 30.
15. Ikemura, K.; Endo, T. *Dent. Mat. J.* **2010**, *29*(5), 481.
16. Drobny, J. G. Radiation Technology for Polymers. 2nd ed.; Taylor & Francis: Baco Raton, FL, **2010**.
17. Fouassier, J.-P.; Lalevée, J. Photoinitiators for Polymer Synthesis; Wiley-VCH: Weinheim, **2012**.
18. Lalevée, J.; Foussier, J.-P. Photopolymerisation Initiating Systems; CPI group: Croydon, **2018**.
19. Kolczak, U.; Rist, G.; Dietliker, K.; Wirz, J. *J. Am. Chem. Soc.* **1996**, *118*, 6477.
20. Liegard, A.; Dietliker, K.; Dubs, P.; Knobloch, G.; Kolczak, U.; Leppard, D.; Martin, R.; Meier, H. R.; Rzadek, P.; Rist, G. *Appl. Magn. Reson.* **1996**, *10*, 395.
21. Kamachi, M.; Kutawa, K.; Sumiyoshi, T.; Schnabel, W. *J. Chem. Soc. Perkin. Trans.* **1988**, *2*, 961.
22. Decker, C.; Zahouily, K.; Decker, D.; Nguyen, T.; Viet, T. *Polymer*. **2001**, *42*, 7551.
23. Jockusch, S.; Koptyug, I. V.; McGarry, P. F.; Sluggett, G. W.; Turro, N. J.; Watkins, D. M. *J. Am. Chem. Soc.* **1997**, *119*, 11495.
24. Majima, T.; Schnabel, W. *J. Photochem.* **1989**, *50*, 31.
25. Scott, T. F.; Cook, W. D.; Forsythe, J. S.; Bowman, C. N.; Berchtold, K. A. *Macromol*. **2003**, *36*, 6066.
26. Sluggett, G. W.; McGarry, P. F.; Koptyug, I. V.; Turro, N. J. *J. Am. Chem. Soc.* **1996**, *118*, 7367.
27. Jockusch, S.; Turro, N. J. *J. Am. Chem. Soc.* **1998**, *120*, 11773.
28. Kolodziejski, W. *Chem. Phys. Lett.* **1979**, *78*(3), 586.
29. Kolodziejski, W.; Kecki, Z. *Chem. Phys. Lett.* **1978**, *54*(2), 286.
30. Waver, I.; Kecki, Z.; Denisow, G. S. J. *Mol. Struct.* **1994**, *327*, 313.
31. Morishima, I.; Endo, K.; Yonezawa, T. *J. Am. Chem. Soc.* **1971**, *93*(8), 2048.
32. Shenderovich, I. G.; Kecki, Z.; Wawer, I.; Denisow, G. S. *Spectrosc. Lett.* **1997**, *30*(8), 1515.
33. Lim, Y. Y.; Drago, R. S. *J. Am. Chem. Soc.* **1971**, *93*(4), 891.
34. Tao, X.; Kehr, G.; Wang, X.; Daniliuc, C. G.; Grimme, S.; Erker, G. *Chem. A Eur. J.* **2016**, *22*, 9504.